Lα, Lβ, and Lγ x-ray production cross sections of Hf, Ta, W, Re, Os, Au, Pb, and Bi by electron impact: Comparison of distorted-wave calculations with experiment

José M. Fernández-Varea, Silvina Segui, and Michael Dingfelder

Phys. Rev. A **83**, 022702 — Published 4 February 2011

DOI: 10.1103/PhysRevA.83.022702

$L\alpha$, $L\beta$, and $L\gamma$ x-ray production cross sections of Hf, Ta, W, Re, Os, Au, Pb, and Bi by electron impact. Comparison of distorted-wave calculations with experiment

José M. Fernández-Varea*

Facultat de Física (ECM and ICC),

Universitat de Barcelona. Diagonal 647, E-08028 Barcelona, Spain

Silvina Segui†

Centro Atómico Bariloche, Comisión Nacional de Energía Atómica. 8400 San Carlos de Bariloche, Río Negro, Argentina

Michael Dingfelder

Department of Physics, East Carolina University. Greenville, North Carolina 27858, USA

Abstract

We study the emission of $L\alpha$, $L\beta$, and $L\gamma$ characteristic x-rays by the impact of electrons on Hf, Ta, W, Re, Os, Au, Pb, and Bi atoms. To this end, ionization cross sections of the L_1, L_2, and L_3 subshells of these atoms are calculated within the distorted-wave Born approximation. The considered energy interval spans from the ionization threshold up to 50 keV. Atomic relaxation parameters (i.e. Coster–Kronig and radiative transition probabilities, fluorescence yields, and emission rates) taken from the literature are then used to evaluate x-ray production cross sections. The theoretical predictions are compared with published experimental information. Good agreement is found for Ta, W, Os, Au, Pb, and Bi. In the case of Hf and Re the measured cross sections are lower than the theoretical estimates by around 30%. The observed discrepancies might be attributed to the methods employed to correct the raw experimental data for the excess of detected characteristic x-rays caused by the finite thickness of the sample's active layer and the presence of the thick substrate.

*jose@ecm.ub.es

†Member of the Consejo Nacional de Investigaciones Científicas y Técnicas (CONICET), Argentina

I. INTRODUCTION

The ionization of atoms by electron impact is a fundamental process of nature. It is therefore not surprising that the theoretical and experimental investigation of electron-atom ionizing collisions has occupied physicists for many decades, and that this topic is still the subject of intense research. When the collision involves a tightly-bound shell the atom may emit, in the course of the subsequent relaxation, a characteristic x-ray whose energy constitutes a fingerprint of the ionized shell and atom. This feature is exploited e.g. in electron-probe microanalysis [1], so that knowledge on inner-shell ionization cross sections is essential for quantitative analysis with this technique. Such data are also needed in medical physics, where diagnostic radiology and mammography demand an accurate modeling of the characteristic x-ray yield by x-ray tubes operated between 20 and 150 kV [2]. Last but not least, the subject of inner-shell ionization by electrons, positrons and heavier charged particles is challenging from a purely theoretical point of view.

The distorted-wave Born approximation (DWBA) is an elaborate *ab initio* method that enables the calculation of cross sections for the ionization of atomic inner shells by electrons (or other charged particles). Computational difficulties limited early applications of this formalism either to differential cross sections [3] or to highly-charged (hydrogenic) atoms [4]. More recent approaches have overcome these problems and provide total ionization cross sections for neutral atoms [5–7]. The theoretical estimates from the DWBA can be compared with measurements of characteristic x-rays emitted after electron impact. To do so, ionization cross sections can be converted into x-ray emission cross sections using atomic relaxation parameters. Previous studies have shown satisfactory agreement between DWBA calculations and several experiments [5, 7–10]. The emphasis was on K-shell ionization of atoms with intermediate or large atomic number Z, and L-shell ionization of intermediate Z. Nevertheless, in order to achieve a thorough assessment of the DWBA it is essential to carry out more extensive comparisons. For instance, the L x-ray lines and line groups of heavy atoms remain largely unexplored. In the present work, $L\alpha$, $L\beta$, and $L\gamma$ x-ray production cross sections of various atoms with $72 \leq Z \leq 83$ are calculated having recourse to the DWBA. The focus is on the near-threshold energy interval where the distortion of the projectile wave function caused by the atomic potential is more pronounced and exchange effects between the incident and target electrons become appreciable, thus posing a stringent

test to the performance of existing theoretical formalisms.

II. IONIZATION AND X-RAY EMISSION CROSS SECTIONS

We have employed the DWBA [5] to calculate the ionization cross sections σ_{L_i} of subshells L_1 ($2s_{1/2}$), L_2 ($2p_{1/2}$), and L_3 ($2p_{3/2}$) of Hf, Ta, W, Re, Os, Au, Pb, and Bi atoms (Z = 72, 73, 74, 75, 76, 79, 82, and 83 respectively). The incident projectiles are electrons with kinetic energy E ranging from the ionization thresholds up to 50 keV. In the adopted implementation of the DWBA, atomic wave functions are evaluated within the independent-electron approximation, so that a single (active) atomic electron is involved in the ionization process. One-electron orbitals are obtained by solving numerically the Dirac equation with self-consistent Dirac–Fock–Slater potentials (correlation effects are relatively unimportant for inner shells). The projectile electron is described employing plane waves which are distorted by the atomic potential. Only the longitudinal part of the interaction between the projectile and the active electron is included in the hamiltonian since the transverse interaction may be disregarded at the relatively low energies addressed in this article. A more detailed account of the DWBA formalism and the associated numerical methods can be found in Refs. [5, 7].

From the calculated σ_{L_i} we have evaluated cross sections $\sigma^{\rm h}_{L_i}$ for the production of vacancies in those subshells through the relations (see e.g. Refs. [10, 11])

$$\sigma^{\rm h}_{L_1} \;=\; \sigma_{L_1}\,, \tag{1}$$

$$\sigma^{\rm h}_{L_2} \;=\; \sigma_{L_2} + f_{12}\,\sigma_{L_1}\,, \tag{2}$$

$$\sigma^{\rm h}_{L_3} \;=\; \sigma_{L_3} + f_{23}\,\sigma_{L_2} + \Big(f_{13} + f'_{13} + f_{12}\,f_{23}\Big)\sigma_{L_1}\,, \tag{3}$$

where f_{ij} and f'_{ij} are, respectively, Coster–Kronig and radiative transition probabilities between subshells L_i and L_j. Notice that in these expressions the contributions due to migration of vacancies from the K shell to the L_i subshells have been omitted because, for the presently investigated atoms, the considered electron energies are lower than the corresponding K-shell binding energies.

Finally, we have obtained cross sections for the production of $L\alpha$, $L\beta$, and $L\gamma$ x-rays by

the studied atoms from equations [10, 11]

$$\sigma^{x}_{L\alpha} = \frac{\Gamma_{3\alpha}}{\Gamma_{3,\mathrm{total}}}\,\omega_3\,\sigma^{\mathrm{h}}_{L_3}, \tag{4}$$

$$\sigma^{x}_{L\beta} = \frac{\Gamma_{3\beta}}{\Gamma_{3,\mathrm{total}}}\,\omega_3\,\sigma^{\mathrm{h}}_{L_3} + \frac{\Gamma_{2\beta}}{\Gamma_{2,\mathrm{total}}}\,\omega_2\,\sigma^{\mathrm{h}}_{L_2} + \frac{\Gamma_{1\beta}}{\Gamma_{1,\mathrm{total}}}\,\omega_1\,\sigma^{\mathrm{h}}_{L_1}, \tag{5}$$

$$\sigma^{x}_{L\gamma} = \frac{\Gamma_{2\gamma}}{\Gamma_{2,\mathrm{total}}}\,\omega_2\,\sigma^{\mathrm{h}}_{L_2} + \frac{\Gamma_{1\gamma}}{\Gamma_{1,\mathrm{total}}}\,\omega_1\,\sigma^{\mathrm{h}}_{L_1}, \tag{6}$$

where ω_i are the fluorescence yields of subshells L_i, whereas $\Gamma_{i\alpha}$, $\Gamma_{i\beta}$, and $\Gamma_{i\gamma}$ are emission rates for transitions belonging to the $L\alpha$, $L\beta$, and $L\gamma$ groups of lines, respectively, and $\Gamma_{i,\mathrm{total}}$ are emission rates for all possible transitions from M and higher shells to subshells L_i. Only dipole-allowed transitions have been included in the $L\alpha$, $L\beta$, and $L\gamma$ x-ray series, as indicated in Table I. On the other hand, transitions from the P subshells were disregarded owing to their negligible contribution to the corresponding x-ray production cross sections.

TABLE I: Single transitions considered in the L series (as given by Bearden [12]), designated with both the conventional (Siegbahn) and IUPAC notations [13].

Series	Transitions
$\Gamma_{3\alpha}$	$L\alpha_{2,1}$ ($L_3M_{4,5}$)
$\Gamma_{3\beta}$	$L\beta_6$ (L_3N_1), $L\beta_{15,2}$ ($L_3N_{4,5}$), $L\beta_7$ (L_3O_1), $L\beta_5$ ($L_3O_{4,5}$)
$\Gamma_{2\beta}$	$L\beta_1$ (L_2M_4)
$\Gamma_{1\beta}$	$L\beta_{4,3}$ ($L_1M_{2,3}$)
$\Gamma_{2\gamma}$	$L\gamma_{5,1}$ ($L_2N_{1,4}$), $L\gamma_8$ (L_2O_1), $L\gamma_6$ (L_2O_4)
$\Gamma_{1\gamma}$	$L\gamma_{2,3}$ ($L_1N_{2,3}$), $L\gamma'_4$ (L_1O_2), $L\gamma_4$ (L_1O_3)
$\Gamma_{i,\mathrm{total}}$	all transitions from the M, N, and O shells to the L_i subshell

We have adopted two sets of atomic relaxation parameters (ω_i, f_{ij}, f'_{13}, Γ_i), hereafter referred to as A and B, in order to estimate their influence on the calculated x-ray production cross sections. The references from which this information has been borrowed are listed in

Table II, and are the same as those utilized in Ref. [10]. Set A is based on the classical compilations of Krause [14] and Scofield [15], and set B consists of purely theoretical estimates [16, 17]; both sets include the radiative transition probabilities from Ref. [14]. For some of the studied elements and x-ray line groups we have considered yet another set, A′, where the ω_i and f_{ij} coefficients of set A are replaced by measured values from Ref. [18].

TABLE II: Atomic relaxation parameters adopted in the present work.

Parameters	Set A	Set B
ω_i	Krause [14]	Campbell [16]
f_{ij}	Krause [14]	Campbell [16]
f'_{13}	Krause [14]	Krause [14]
Γ_i	Scofield [15]	Campbell and Wang [17]

III. RESULTS AND DISCUSSION

The $L\alpha$, $L\beta$, and $L\gamma$ x-ray production cross sections for Hf, Ta, W, Re, Os, Au, Pb, and Bi are shown in Figs. 1–8. The theoretical values, calculated as summarized above with the DWBA and the relaxation data from sets A, B, and A′ are plotted as continuous, dashed, and dot-dashed curves, respectively. Experimental x-ray emission cross sections reported in the literature [19–27] are depicted as symbols with their respective uncertainty bars. Most of these measurements have been performed very recently at Sichuan University.

Regarding the present theoretical calculations it can be seen that, for the $L\alpha$ and $L\beta$ lines of the investigated atoms, x-ray emission cross sections computed from relaxation parameter sets A and B differ by at most 6%. The predictions for the $L\gamma$ cross sections obtained using the same data sets display somewhat larger differences, namely 10–15%. In turn, experimental uncertainties are typically about 10–20%. As a consequence, the overall rather limited discrepancies between x-ray production cross sections evaluated from the DWBA ionization cross sections facilitate a meaningful assessment of the DWBA results.

Agreement between our theoretical calculations and the experimental data from the quoted references is excellent for Ta, Os, Au, Pb, and Bi (Figs. 2, 5, 6, 7, and 8, respectively). This is especially noteworthy in the case of the $L\alpha$ and $L\beta$ lines of Au, for which at

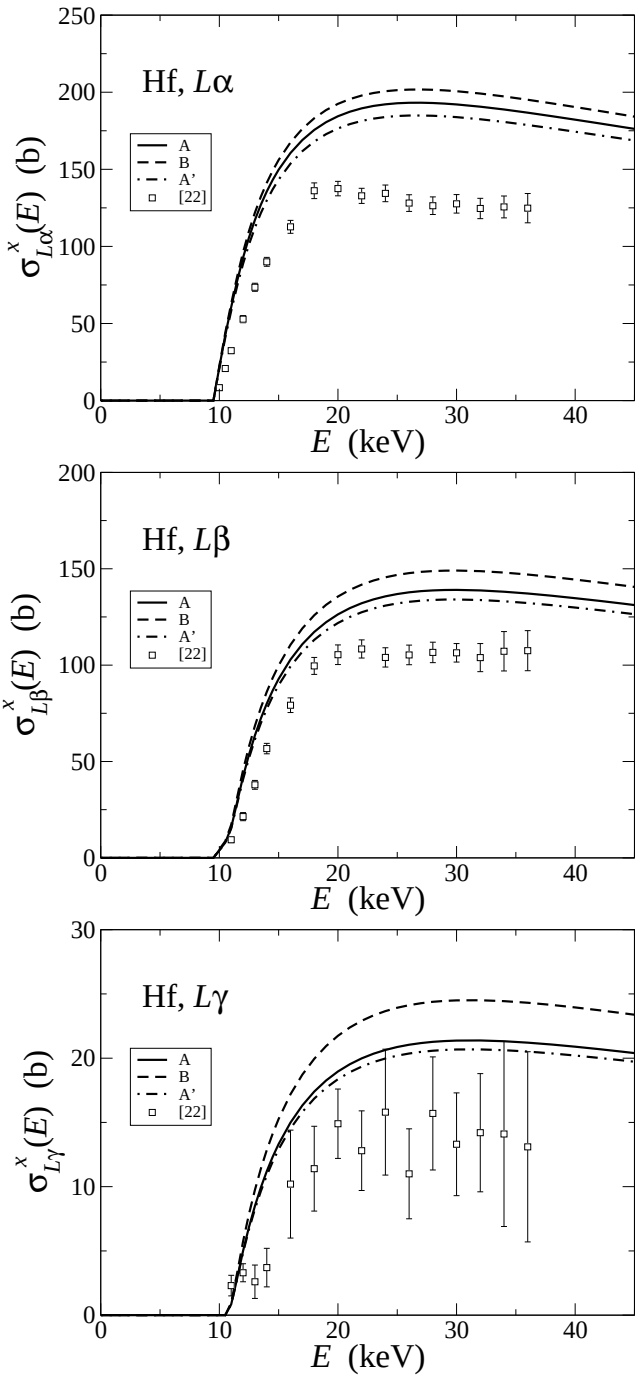

FIG. 1: X-ray production cross sections $\sigma^x_{L\alpha}$, $\sigma^x_{L\beta}$, and $\sigma^x_{L\gamma}$ of Hf as a function of energy. The continuous, dashed, and dot-dashed curves correspond to the theoretical cross sections calculated with sets A, B, and A$'$, respectively. Symbols are experimental data from Ref. [22].

least two independent sets of measurements exist. Wu *et al* [27] have already pointed out that the DWBA $L\alpha$ and $L\beta$ x-ray production cross sections of Bi compare quite well with

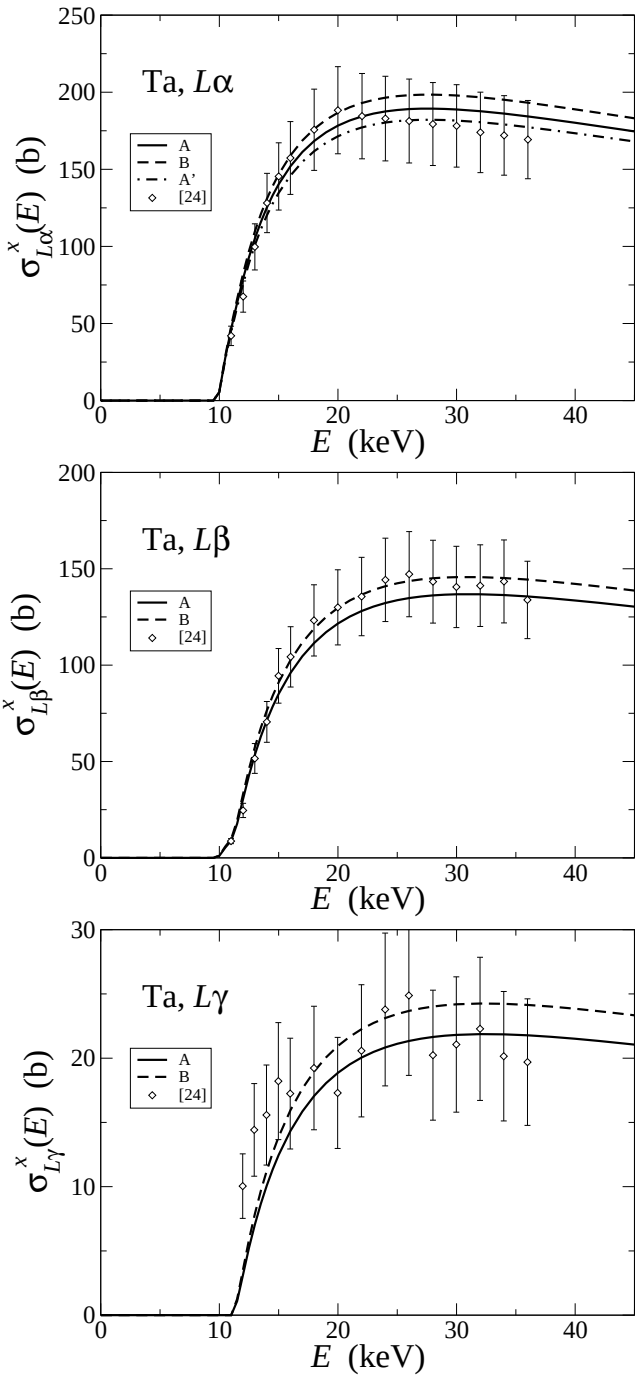

FIG. 2: X-ray production cross sections $\sigma^x_{L\alpha}$, $\sigma^x_{L\beta}$, and $\sigma^x_{L\gamma}$ of Ta as a function of energy. The continuous, dashed, and dot-dashed curves correspond to the theoretical cross sections calculated with sets A, B, and A′ (only $L\alpha$), respectively. Symbols are experimental data from Ref. [24].

their experimental values. In the analysis these authors used atomic relaxation data from Refs. [16, 17] (i.e. set B).

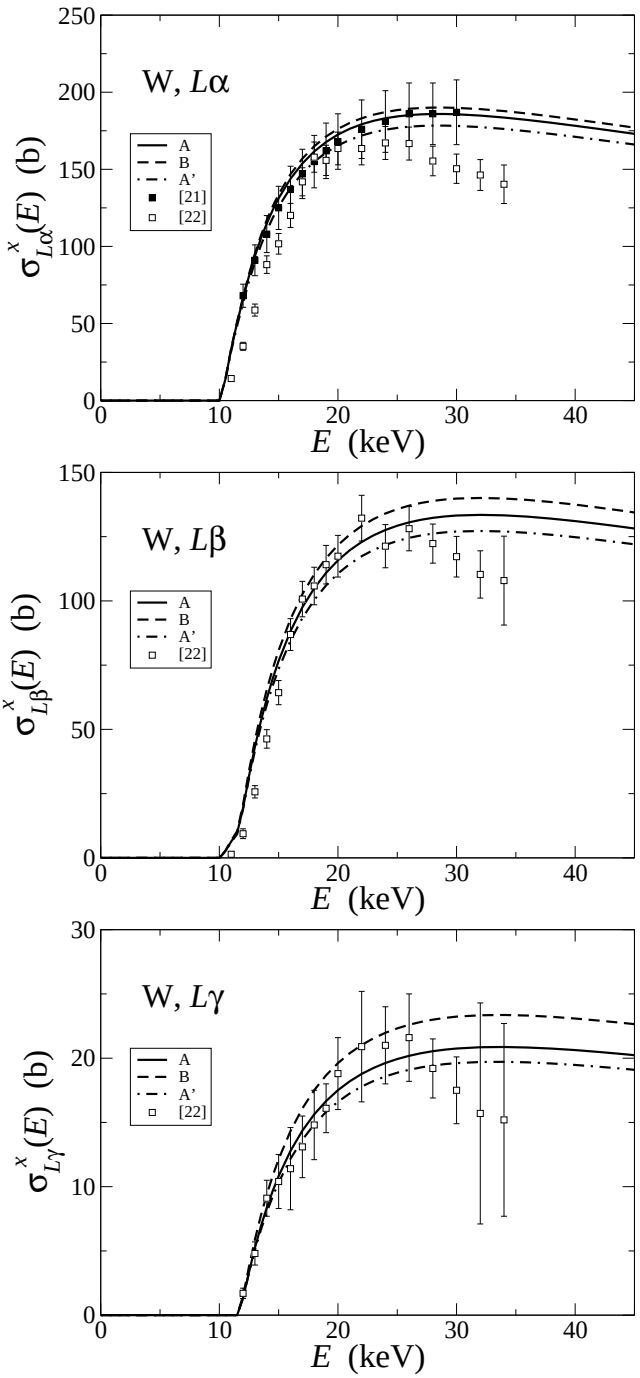

FIG. 3: X-ray production cross sections $\sigma^x_{L\alpha}$, $\sigma^x_{L\beta}$, and $\sigma^x_{L\gamma}$ of W as a function of energy. The continuous, dashed, and dot-dashed curves correspond to the theoretical cross sections calculated with sets A, B, and A′, respectively. Symbols are experimental data from Refs. [21, 22].

Theoretical and measured x-ray emission cross sections of W (Fig. 3) are in good accord for the lower energies, but the data of Ref. [22] fall off somewhat more rapidly above 25 keV.

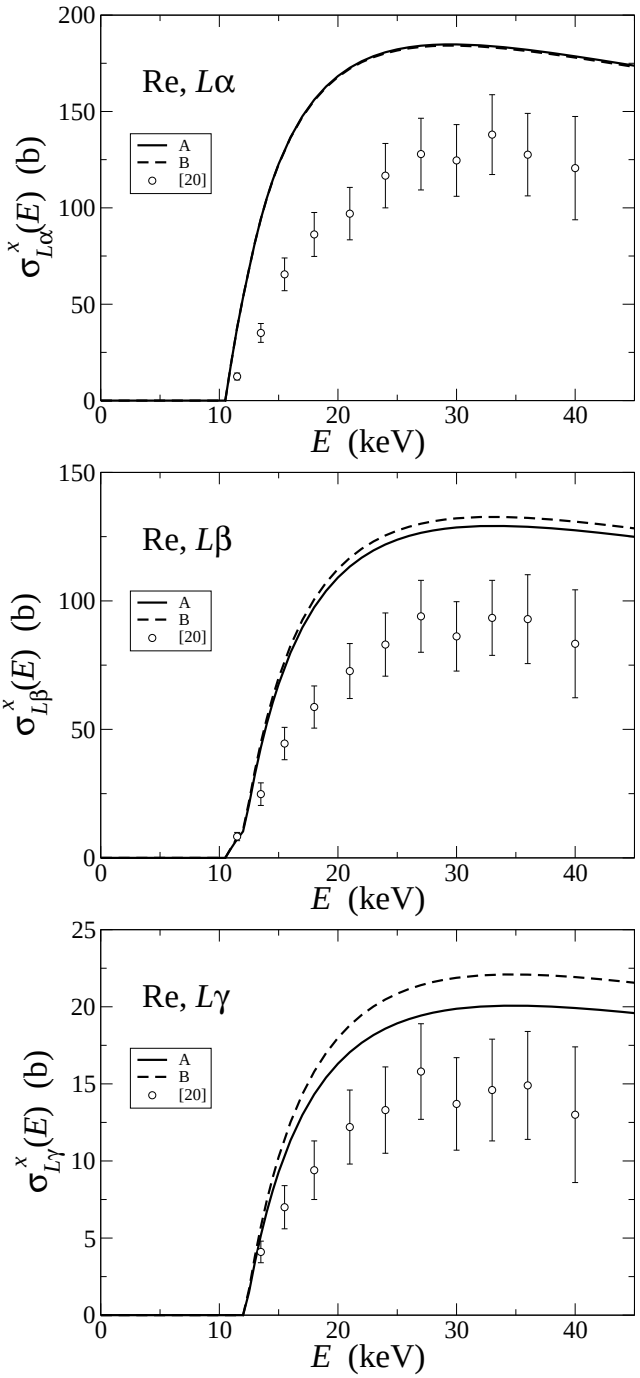

FIG. 4: X-ray production cross sections $\sigma^x_{L\alpha}$, $\sigma^x_{L\beta}$, and $\sigma^x_{L\gamma}$ of Re as a function of energy. The continuous and dashed curves correspond to the theoretical cross sections calculated with sets A and B, respectively. Symbols are experimental data from Ref. [20].

This mismatch is probably not significant because the experimental $L\alpha$ cross sections of Ref. [21] do not show that behavior. Further support for larger x-ray emission cross sections

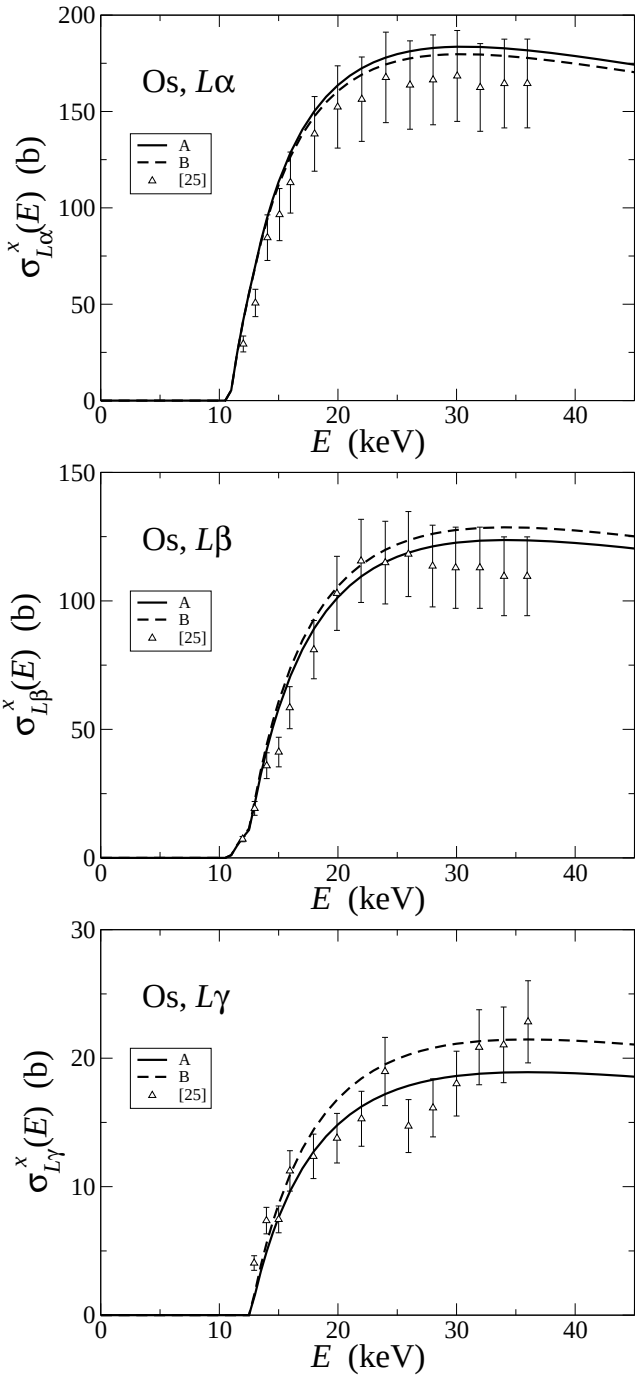

FIG. 5: X-ray production cross sections $\sigma^x_{L\alpha}$, $\sigma^x_{L\beta}$, and $\sigma^x_{L\gamma}$ of Os as a function of energy. The continuous and dashed curves correspond to the theoretical cross sections calculated with sets A and B, respectively. Symbols are experimental data from Ref. [25].

is provided by the measurements of Ref. [28]. Note also that the uncertainty bars of the $L\gamma$ line are rather large at the highest energies considered.

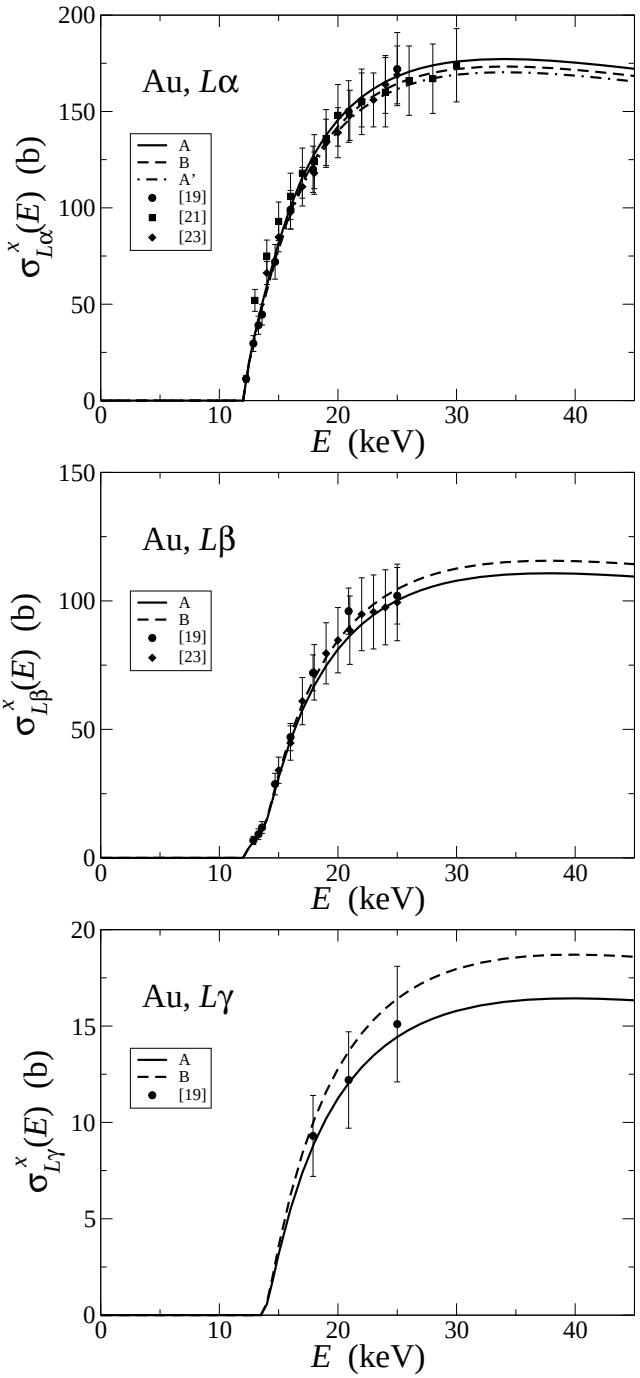

FIG. 6: X-ray production cross sections $\sigma^x_{L\alpha}$, $\sigma^x_{L\beta}$, and $\sigma^x_{L\gamma}$ of Au as a function of energy. The continuous, dashed, and dot-dashed curves correspond to the theoretical cross sections calculated with sets A, B, and A$'$ (only $L\alpha$), respectively. Symbols are experimental data from Refs. [19, 21, 23].

The situation is less satisfactory for Hf and Re (Figs. 1 and 4, respectively), where the

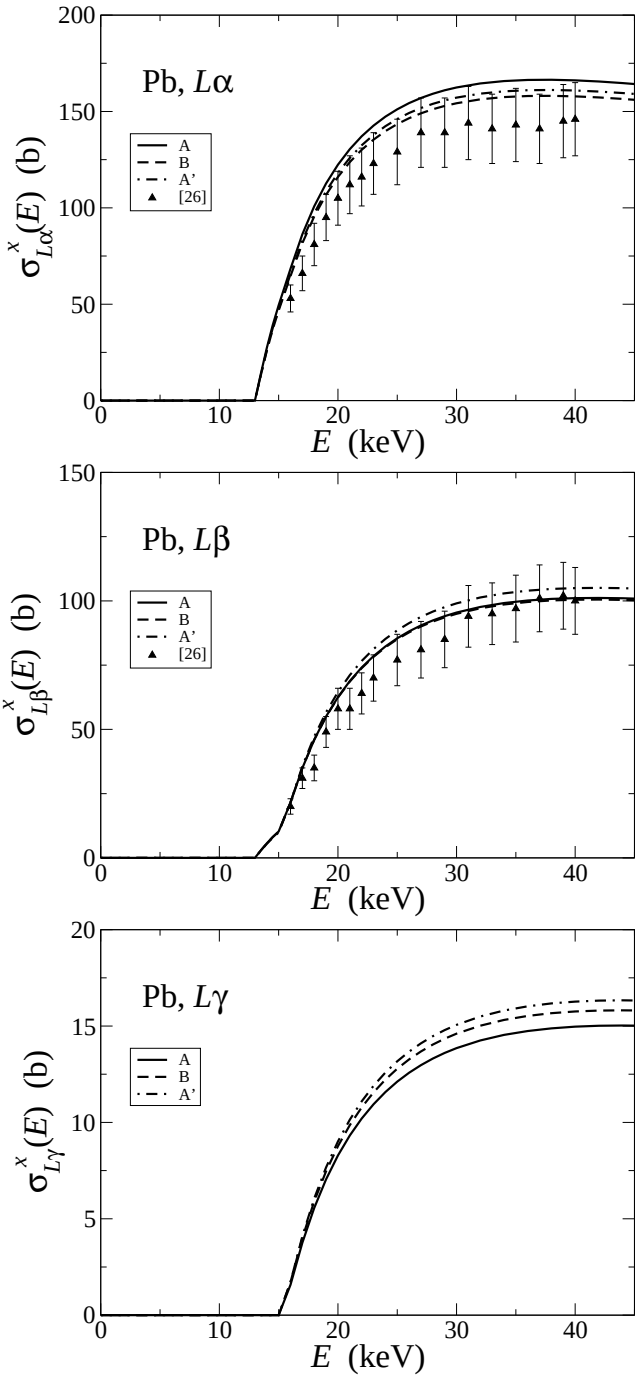

FIG. 7: X-ray production cross sections $\sigma^x_{L\alpha}$, $\sigma^x_{L\beta}$, and $\sigma^x_{L\gamma}$ of Pb as a function of energy. The continuous, dashed, and dot-dashed curves correspond to the theoretical cross sections calculated with sets A, B, and A′, respectively. Symbols are experimental data from Ref. [26].

theoretical cross sections are systematically around 30% larger than the data of Refs. [20, 22]. The largest disagreement is seen for the $L\alpha$ x-rays of these two atomic species.

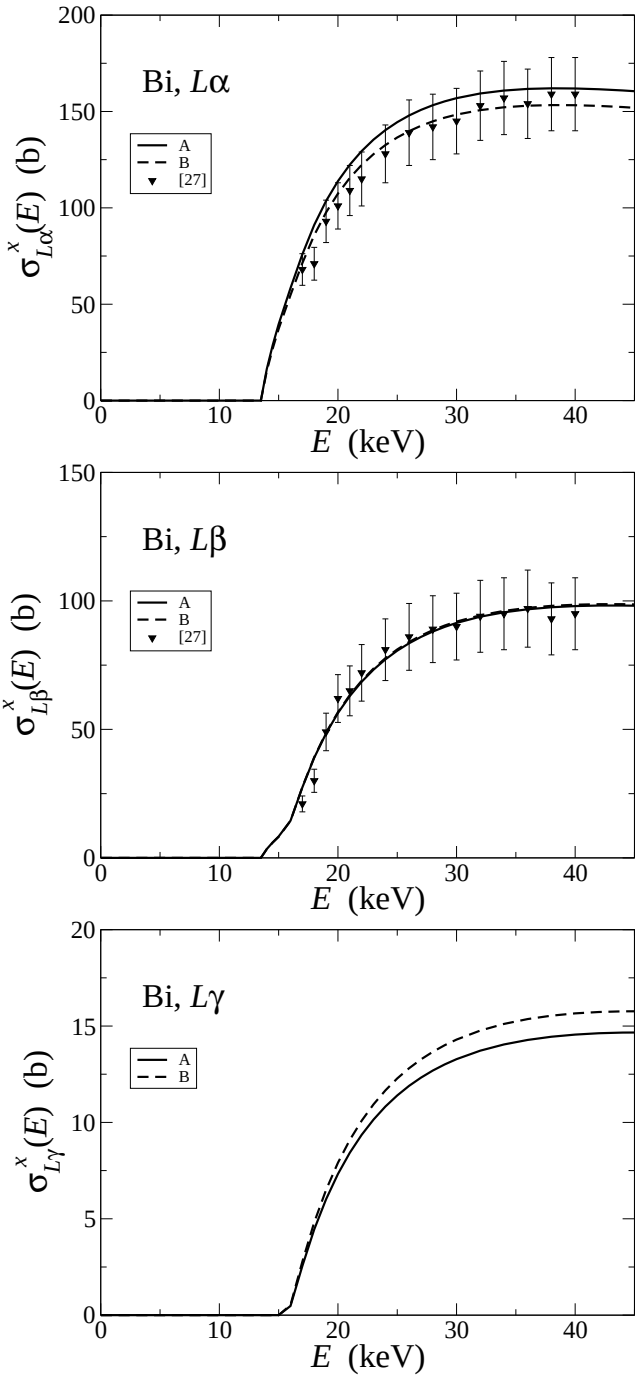

FIG. 8: X-ray production cross sections $\sigma^x_{L\alpha}$, $\sigma^x_{L\beta}$, and $\sigma^x_{L\gamma}$ of Bi as a function of energy. The continuous and dashed curves correspond to the theoretical cross sections calculated with sets A and B, respectively. Symbols are experimental data from Ref. [27].

Notice that the curves pertaining to the $L\beta$ lines show, slightly above the threshold, a discontinuity in the derivative. This is due to the fact that the three L_i subshells contribute

to the $L\beta$ group, see Eq. (5) and Table I, each one with its own ionization threshold. This feature is particularly well reproduced by the calculations in the cases of Os and Au, for which the agreement with the data from Refs. [25] and [23], respectively, is remarkable. On the other hand, the discontinuity in the derivative of the $L\gamma$ x-ray emission cross sections is less pronounced because for heavy atoms the binding energies of the involved L_1 and L_2 subshells are close to each other (whereas the binding energy of the L_3 subshell is considerably lower) as the atomic potential experienced by the electrons in deep inner shells is nearly Coulombian.

In the case of Hf, Ta, W, Au, and Pb the corresponding figures include x-ray emission cross sections calculated with set A′, i.e. using the fluorescence yields and Coster–Kronig coefficients measured by Werner and Jitschin resorting to the accurate synchrotron photoionization method [18]. There is only minor improvement in the accord between theoretical x-ray emission cross sections and experiment. Although the uncertainties introduced by the choice of relaxation parameters are not negligible for the presently-studied elements, they do not account for the large differences observed for Hf and Re. It seems more plausible that difficulties in the experiments conducted to measure x-ray production cross sections or, more likely, in the subsequent processing of the raw experimental data might explain the lack of agreement. In the following paragraphs we discuss some issues that could affect the present comparison.

Substantial uncertainties are sometimes associated to the thickness of the irradiated samples. For instance, an uncertainty of 10% was reported for Re [20], but a figure of 5% was quoted for Hf [22] and most of the studied elements. Anyhow, uncertainties much larger than 10% in the determination of the sample thickness would be required to justify the absence of agreement observed for Hf and Re, but this appears improbable.

Another source of problems could lie in the detection of x-rays. The energy resolution of the Si(Li) detectors commonly used, around 150–200 eV at 5.9 keV, is enough to resolve the $L\alpha$, $L\beta$, and $L\gamma$ line groups in the recorded x-ray spectra. This helps limiting the uncertainty related to the evaluation of peak areas (unlike what happens for atoms with intermediate Z, where the various L lines may overlap). Besides, the efficiency of the Si(Li) spectrometers is almost constant in the photon energy interval of interest in this work and it can be known with good accuracy. The uncertainty in the statistics of the net x-ray count (i.e. after removing the bremsstrahlung background in the peaks) is usually kept reasonably low.

Finally, we address the processing of the raw experimental data, which is straightforward only if the monoenergetic electron beam impinges on a very thin, self-supporting film of the active element. The reason is that the number of recorded characteristic x-rays of a given line or line group is then proportional to the corresponding x-ray production cross section. However, to avoid the complications inherent to the manufacture of such demanding films, most researchers (cf. e.g. [9]) prepare instead samples in the form of a (not so) thin layer of the active element deposited on a thick substrate, see Table III. Elastic scattering of electrons in the active layer increases the path length of the electron beam. Moreover, electrons backscattered from the substrate with sufficient energy induce further ionizations of the considered (sub)shells of the active element. Both effects combine to yield an excess of characteristic x-rays in the acquired spectra, which is magnified if the electron beam impinges on the sample with a tilted angle. Consequently, the recorded raw data must be corrected for this surplus of x-rays. The method adopted to subtract the spurious x-ray contribution does introduce additional uncertainties in the resulting experimental x-ray production cross sections. These type B uncertainties are difficult to quantify and may easily be underestimated. We suspect that the origin of the surprisingly large discrepancies between theory and experiment found for Hf and Re could be partly ascribed to the corrections employed to compensate the measurements for the finite thickness of the active layer and for the presence of the substrate.

The two effects that contribute to the excess of x-rays have often been treated separately. Firstly, the effective path length of the electrons in the active layer can be estimated through Monte Carlo simulations. For instance, the EGS4 code [29] was used in the determination of cross sections of Hf and W [22]. It is known that the Molière multiple-scattering theory implemented in EGS4 to describe elastic collisions fails at the short step lengths and rather low energies presently addressed (see e.g. Ref. [30]), so that the ensuing path-length corrections could be affected by errors which are important if the active layer is not too thin, e.g. for Hf. In other cases no path-length correction was applied (Re and Os) [20, 25] or the employed method was not described (Ta) [24]. Secondly, the correction for the electrons backscattered from the substrate has been evaluated in Refs. [20, 22, 24, 25] having recourse to the so-called bipartition model [31] and an iterative procedure [32]. The bipartition model is also based on multiple-scattering theory and thus may lose accuracy when applied to the energies of present concern. However, the Al substrate on which W was deposited in the

TABLE III: Element and mass thickness of the active layer and substrate in the samples prepared for the analyzed experiments. α is the incidence angle of the electron beam with respect to the normal of the sample surface. Where two corrections are given, the first one refers to the method used to evaluate the effective path length in the active layer whereas the second one pertains to the way the contribution of electrons reflected from the substrate is estimated; BM stands for bipartition model.

Target		Substrate		α /deg	Correction(s)	Ref.
Element	$\rho_t t_t$ /μg cm^{-2}	Element	$\rho_s t_s$ /mg cm^{-2}			
Hf	29.4	Al	1.84	45	EGS4 + BM	[22]
Ta	19.7	Al	4.07	45	? + BM	[24]
W	14.5	C	thick	0	PENELOPE	[21]
W	28.8	Al	0.06	45	EGS4 + BM	[22]
Re	34.5	Al	thick	45	none + BM	[20]
Os	15.3	Al	4.31	45	none + BM	[25]
Au	13.7	C	thick	0	PENELOPE	[21]
Au	11.1	Al	thick	45	PENELOPE	[23]
Pb	10.5	C	thick	45	PENELOPE	[26]
Bi	10.7	C	thick	45	PENELOPE	[27]

experiment reported in Ref. [22] was so thin (see Table III) that the possible shortcomings of the bipartition model could be less noticeable owing to the smallness of the correction.

Alternatively, a global correction factor f_c can be determined by Monte Carlo simulations as proposed by Campos *et al* [21]. This method is *a priori* more suitable provided the adopted code implements accurate electron interaction models. Incidentally, a practical advantage is that a single simulation is enough to get f_c for each energy, i.e. the need of an iterative procedure is circumvented. The general-purpose Monte Carlo code PENELOPE [33] has been routinely used in Refs. [21, 23, 26, 27] to estimate f_c (or $K = 1 - f_c^{-1}$ in the terminology of Refs. [23, 26, 27]).

In summary, the best accordance between the theoretical DWBA x-ray production cross sections and experiment happens for the thinnest targets and when a global factor deter-

mined from Monte Carlo simulations is utilized to compensate for the excess of characteristic x-rays in the recorded spectra. The use of a low-Z element like C for the substrate and a setup where the electron beam impinges perpendicularly on the sample are conditions that render values of f_c close to 1, thus minimizing the influence of the correction on the resulting x-ray production cross sections.

IV. CONCLUSIONS

We have employed the DWBA to calculate L_1, L_2, and L_3 ionization cross sections of Hf, Ta, W, Re, Os, Au, Pb, and Bi by the impact of electrons with energies near the ionization threshold. Three sets of atomic relaxation parameters were chosen to convert ionization to x-ray emission cross sections. The latter have been compared with experimental values from the literature. Agreement between theory and measurements is quite good in the case of Ta, W, Os, Au, Pb, and Bi. However, discrepancies of about 30% are found for Hf and Re.

The theoretical x-ray production cross sections obtained with the three data sets of relaxation parameters generally differ by less than around 10%, suggesting that for the investigated heavy elements the conversion of ionization to x-ray emission cross sections is not too sensitive to the election of relaxation parameters. We then speculate on the importance of the method to subtract the excess of characteristic x-rays that are emitted by a sample consisting of a thin layer of the active element on a thick substrate. The specific corrections used in the experiments where the x-ray production cross sections of Hf and Re were measured, namely a path-length correction derived from EGS4 Monte Carlo simulations plus a calculation based on the bipartition model to account for electrons reflected from the substrate, might be partly responsible for the found disagreement.

Further support for the accuracy of the DWBA x-ray production cross sections for heavy elements is provided by experiments where characteristic x-rays emitted from thick samples subjected to electron bombardment are recorded. Shima *et al* [28] measured $L\alpha$ x-ray yields from bulk Sn, Sm, Ta, W, Pt, Au, and Pb irradiated by electron beams with energies up to 30 keV. Their experimental values are in accord with the results of Monte Carlo simulations carried out with the PENELOPE code [34], which implements DWBA cross sections to describe the ionization of atomic inner shells (and relaxation parameters from the Evaluated Atomic Data Library).

Finally, we would like to mention the scarcity of experimental cross sections for the ionization of M subshells. In this context, Merlet *et al.* [35] have reported very good agreement between their measured $M\alpha$ x-ray production cross sections of Au and Bi and the predictions of the DWBA, a finding that gives additional confidence in this theoretical formalism.

Acknowledgments

We are indebted to Prof. Z. An (Sichuan University) for providing us with their experimental data for W in numerical form, and to Dr. X. Llovet (Barcelona University) for clarifying discussions. J. M. Fernández-Varea thanks the financial support from the Spanish Ministerio de Ciencia e Innovación (projects no. FPA2006-12066 and FPA2009-14091-C02-01) and FEDER as well as the Generalitat de Catalunya (project no. 2009 SGR 276). S. Segui expresses her gratitude to CONICET for an external scholarship. M. Dingfelder acknowledges partial funding from the National Aeronautics and Space Administration (Grant no. NNJ04HF39G).

---

[1] V. D. Scott, G. Love, and S. G. B. Reed, Quantitative Electron-probe Microanalysis (Harwood, New York, 1995).

[2] M. R. Ay, S. Sarkar, M. Shahriari, D. Sardari, and H. Zaidi, Med. Phys. **32**, 1660 (2005).

[3] D. H. Madison, I. E. McCarthy, and X. Zhang, J. Phys. B: At. Mol. Opt. Phys. **22**, 2041 (1989).

[4] M. S. Pindzola, D. L. Moores, and D. C. Griffin, Phys. Rev. A **40**, 4941 (1989).

[5] S. Segui, M. Dingfelder, and F. Salvat, Phys. Rev. A **67**, 062710 (2003).

[6] J. Colgan, C. J. Fontes, and H. L. Zhang, Phys. Rev. A **73**, 062711 (2006).

[7] D. Bote and F. Salvat, Phys. Rev. A **77**, 042701 (2008).

[8] C. Merlet, X. Llovet, and F. Salvat, Phys. Rev. A **69**, 032708 (2004).

[9] C. Merlet, X. Llovet, and J. M. Fernández-Varea, Phys. Rev. A **73**, 062719 (2006); **74**, 049901(E) (2006).

[10] M. Dingfelder, S. Segui, and J. M. Fernández-Varea, Phys. Rev. A **77**, 062710 (2008).

[11] G. W. Baxter and B. M. Spicer, Aust. J. Phys. **36**, 287 (1983).

[12] J. A. Bearden, Rev. Mod. Phys. **39**, 78 (1967).

[13] R. Jenkins, R. Manne, R. Robin, and C. Senemaud, Pure Appl. Chem. **63**, 735 (1991).

[14] M. O. Krause, J. Phys. Chem. Ref. Data **8**, 307 (1979).

[15] J. H. Scofield, At. Data Nucl. Data Tables **14**, 121 (1974).

[16] J. L. Campbell, At. Data Nucl. Data Tables **85**, 291 (2003).

[17] J. L. Campbell and J. -X. Wang, At. Data Nucl. Data Tables **43**, 281 (1989).

[18] U. Werner and W. Jitschin, Phys. Rev. A **38**, 4009 (1988).

[19] K. Shima, T. Nakagawa, K. Umetani, and T. Mikumo, Phys. Rev. A **24**, 72 (1981).

[20] C. Tang, Z. Luo, Z. An, F. He, X. Peng, and X. Long, Phys. Rev. A **65**, 052707 (2002).

[21] C. S. Campos, M. A. Z. Vasconcellos, X. Llovet, and F. Salvat, Phys. Rev. A **66**, 012719 (2002).

[22] D. L. Yang, X. B. Luo, Y. C. Fu, F. Q. He, X. G. Long, X. F. Peng, and Z. M. Luo, Chin. Phys. **13**, 670 (2004).

[23] Y. Wu, Z. An, M. T. Liu, Y. M. Duan, C. H. Tang, and Z. M. Luo, J. Phys. B: At. Mol. Opt. Phys. **37**, 4527 (2004).

[24] Z. -W. Wu, C. -J. Gou, D. -L. Yang, Z. An, X. -F. Peng, F. -Q. He, and Z. -M. Luo, Chin. Phys. Lett. **22**, 2538 (2005).

[25] Z. Wu, C. Gou, D. Yang, X. Peng, F. He, and Z. Luo, Chin. Sci. Bull. **51**, 1929 (2006).

[26] Y. Wu, Z. An, Y. M. Duan, M. T. Liu, and C. H. Tang, J. Phys. B: At. Mol. Opt. Phys. **40**, 735 (2007).

[27] Y. Wu, Z. An, Y. M. Duan, and M. T. Liu, Nucl. Instrum. Meth. B **268**, 2473 (2010).

[28] K. Shima, M. Okuda, E. Suzuki, T. Tsubota, and T. Mikumo, J. Appl. Phys. **54**, 1202 (1983).

[29] W. R. Nelson, H. Hirayama, and D. W. O. Rogers, *The EGS4 Code System*, Report SLAC-265 (Stanford Linear Accelerator Center, Stanford, CA, 1985).

[30] J. M. Fernández-Varea, R. Mayol, J. Baró, and F. Salvat, Nucl. Instrum. Meth. B **73**, 447 (1993).

[31] Z. -M. Luo, Phys. Rev. B **32**, 824 (1985).

[32] Z. Luo, Z. An, F. He, T. Li, X. Long, and X. Peng, J. Phys. B: At. Mol. Opt. Phys. **29**, 4001 (1996).

[33] F. Salvat, J. M. Fernández-Varea, and J. Sempau, *PENELOPE-2008: A Code System*

for Monte Carlo Simulation of Electron and Photon Transport (OECD/NEA, Issy-les-Moulineaux, 2008).

[34] D. Bote, X. Llovet, and F. Salvat, J. Phys. D: Appl. Phys. **41**, 105304 (2008).

[35] C. Merlet, X. Llovet, and F. Salvat, Phys. Rev. A **78**, 022704 (2008).